JOURNAL OF GEOPHYSICAL RESEARCH, VOL. 96, NO. E5, PAGES 22,765–22,776, DECEMBER 25, 1991

The Particle Size of Martian Aeolian Dunes

KENNETH S. EDGETT AND PHILIP R. CHRISTENSEN

Department of Geology, Arizona State University, Tempe

The effective particle size of unconsolidated materials on the Martian surface can be determined from thermal inertia, due to a pore size dependence of thermal conductivity at Martian atmospheric pressures. Because dunes consist of a narrow range of well-sorted, unconsolidated particles, they provide for a test of the relationship between particle size and thermal inertia calculated from midinfrared emission data for the Martian surface. We use two independent approaches. First, thermal inertia data indicate that Martian dunes have an average particle size of about 500 ± 100 μm, or medium to coarse sand. Second, we determine expected dune particle sizes from grain trajectory calculations and the particle size transition from suspension to saltation. On Earth, the transition occurs for a grain when the ratio of the terminal fall velocity to the wind friction speed (u_{*t}) is near unity; for grains at u_{*t}, this occurs at about 52 μm. Terrestrial dune sands have a mean of 250 μm and are composed entirely of grains > 52 μm. The corresponding Martian transition grain size is about 210 μm, suggesting that Martian dunes should be significantly coarser than terrestrial dunes. Grain saltation path length as a function of particle size also shows that under Martian conditions, larger grains than on Earth will become suspended. Both approaches indicate that Martian dune sand should be coarser than terrestrial dune sand. Thus, while terrestrial dune grains are in the fine to medium sand range, the average Martian dune sediments are probably medium to coarse sands. These results closely match the grain sizes determined from thermal inertia models, providing the first direct test of the validity of these models for actual Martian surface materials.

1. INTRODUCTION

Aeolian dunes occur in a variety of locations on Mars, especially in the circum-north polar region [*Cutts et al.*, 1976; *Tsoar et al.*, 1979], on the floors of some craters [e.g., *Cutts and Smith*, 1973; *Breed*, 1977; *Thomas*, 1981, 1982, 1984], and in a variety of locations seen at very high resolution [e.g., *Peterfreund*, 1981; *Zimbelman*, 1987]. Dune fields large enough to have been seen by spacecraft cover at least 0.5% of the Martian surface [*Peterfreund et al.*, 1981]. The morphologies of the Martian dunes are similar to terrestrial dunes and are generally thought to form from saltated grains [*Cutts and Smith*, 1973; *Breed*, 1977; *Breed et al.*, 1979]. On Earth, most aeolian dunes are composed of moderate to well-sorted, fine to medium sand [*Ahlbrandt*, 1979]. The mean particle size of terrestrial dune sand is about 250 μm, with a range of means for various dune fields from 100 to 1600 μm (means calculated for 191 terrestrial dune and interdune areas listed by *Ahlbrandt* [1979]).

The determination of the average Martian dune particle size will serve as a direct test of the relationship between thermal inertias calculated from midinfrared emission observations using thermal models [*Kieffer et al.*, 1977; *Haberle and Jakosky*, 1991]. The thermal inertia as a function of particle size relationship has been determined from laboratory measurements [see *Wechsler and Glaser*, 1965; *Kieffer et al.*, 1973]. Provided that Martian dunes are unconsolidated to at least a depth of 10 cm, they are the most ideal Martian surface material for this test, because dunes are typically composed of a narrow range of particle sizes (for example, on Earth, dunes are composed mainly of particles in the sand size range; 62.5-2000 μm on the *Wentworth* [1922] scale). A second reason for examining the particle sizes of Martian dunes is to compare them with their terrestrial counterparts.

The question of Martian dune particle size is addressed by two different approaches. The first is to examine thermal emission data obtained by the Viking Infrared Thermal Mapper (IRTM) in order to calculate the thermal inertia of Martian dune fields. As explained below, thermal inertia is related to the particle size of unconsolidated deposits at Martian atmospheric pressures. The second approach is to consider the physics of aeolian sediment transport under Martian conditions. Dunes are composed of grains which move primarily by saltation and some via traction [e.g., *Chepil and Woodruff*, 1963, p. 248]. Very few suspendable grains (<< 1%) are found in active dunes. Therefore, establishing the upper limit (in terms of particle size) for suspendable grains will establish a lower limit on dune particle sizes.

Throughout this paper, the following conventions are used: (1) The term "dunes" refers to aeolian dunes only. "Dune field" refers to an areal grouping of dunes. (2) Particle sizes are given in terms of an effective grain diameter in units of microns (μm) and in terms of the *Wentworth* [1922] classification scheme (e.g., medium sand = 250 to 500 μm). (3) Thermal inertia (I) is expressed in units of 10^{-3} cal cm^{-2} s$^{-0.5}$ °K^{-1} (S.I. units = 41.8 J m^{-2} s$^{-0.5}$ °K^{-1}), following the precedent of *Kieffer et al.* [1977], *Palluconi and Kieffer* [1981], and others.

2. PARTICLE SIZES FROM THERMAL INERTIA

Thermal Inertia and Particle Size Relationship

Thermal inertia is a measure of the resistance of a material to a change in temperature. The thermal inertia of a material (I) is defined as $I = (kpc)^{0.5}$, in which k is the thermal conductivity, ρ is the density, and c is the specific heat. The density and specific heat of geologic materials vary by only about a factor of 3; while under Martian conditions, thermal conductivity varies by an order of magnitude [*Neugebauer et al.*, 1971]. Figure 1, adapted from *Wechsler and Glaser* [1965], shows the relationship between thermal conductivity and gas pressure for several particle sizes (D_p), demonstrating the variation of thermal conductivity with particle size at Martian atmospheric pressures (mean ~ 6.5 mbar) [also see *Liu and Dobar*, 1964; *Fountain and West*, 1970; *Wechsler et al.*, 1972]. Particulates have a higher thermal conductivity when the gas mo-

Paper number 91JE02412.
0148-0227/91/91JE-02412$05.00

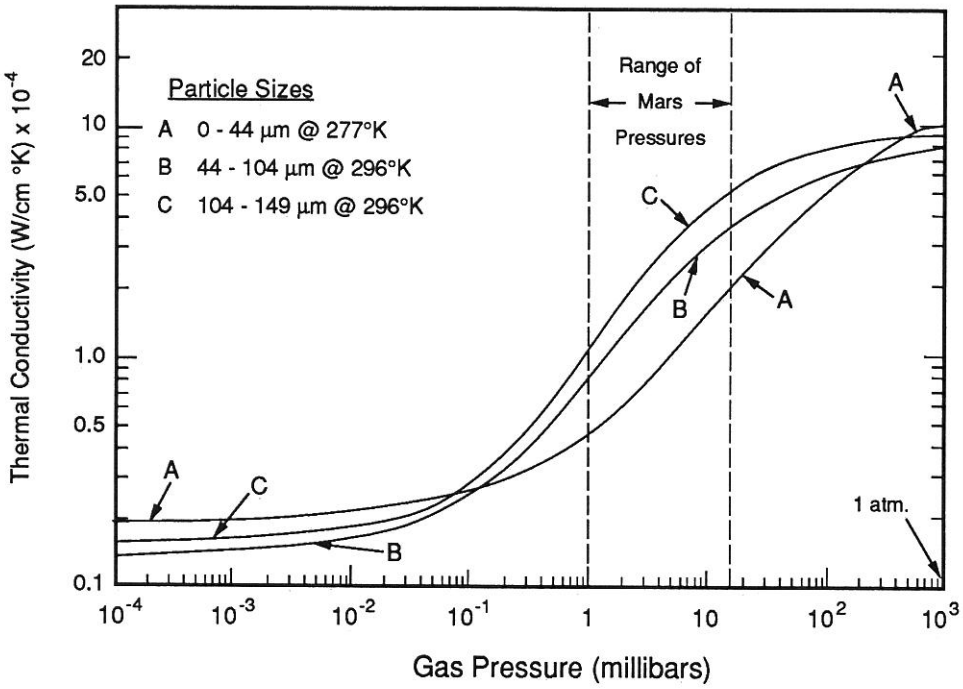

Fig. 1. Thermal conductivity versus gas pressure for several particle size ranges, showing that the greatest separation in the thermal conductivities for unconsolidated particulates occurs at Martian surface atmospheric pressures. The data used to obtain the curves shown here were for pumice grains [*Liu and Dobar*, 1964; *Wechsler and Glaser*, 1965], but data for granular basalt, granite, and glass beads have similar trends [*Masamune and Smith*, 1963; *Wechsler and Glaser*, 1965]. There is a decreased separation in the range of thermal conductivity for particles at terrestrial atmospheric pressure (~10^3 mbar), where gas conduction is the largest contributor to the thermal conductivity of particulates in all size ranges. Also note the decreased separation in the range of thermal conductivity for materials at low, near-vacuum pressures, where solid conduction dominates. (Modified after *Wechsler and Glaser* [1965, Figure 10] with permission from Academic Press and P.E. Glaser.)

lecular mean free path (mfp) is less than the pore size (P_s) between grains (mfp ≈ 5 μm at 6.5 mbar). When mfp > P_s, solid (grain-to-grain) conduction dominates. Pore size is directly related to particle size (D_p) for ideal, spherical particles such that $P_s \approx D_p/100$ [*Woodside and Messmer*, 1961, p. 1698]. Because thermal inertia (I) is largely a function of k, and k is a function of P_s (or D_p) at Martian atmospheric pressures (Figure 1), thermal inertia on Mars is also a function of particle size [*Neugebauer et al.*, 1971; *Kieffer et al.*, 1973].

Figure 2 shows thermal inertia as a function of particle size for Martian conditions. Figure 2 is adapted from *Kieffer et al.* [1973, Figure 11]. The vertical bars, box, two dots, and the triangle (Figure 2) represent thermal inertias calculated from thermal conductivity data (at 6.5 mbar pressure) [*Woodside and Messmer*, 1961; *Masamune and Smith*, 1963; *Wechsler and Glaser*, 1965; *Fountain and West*, 1970]. These data and the dark, central curve in Figure 2 represent materials for which $\rho c = 0.24$ cal °K^{-1} cm^{-3}, which was derived from arguments, presented by *Neugebauer et al.* [1971], that surface material densities (ρ) on Mars probably range from 1.3 to 2.0 g/cm^3 and that the specific heat (c) of most minerals is approximately 0.19 cal g^{-1} °K^{-1} at 300°K [e.g., *Muhleman*, 1972, Figure 5], which would be about 0.16 cal g^{-1} °K^{-1} at lower, Martian temperatures (note that Neugebauer et al. referred to a paper by S.W. Kieffer and B. Kamb (unpublished manuscript, 1971) for the specific heat value; this paper was never published in its 1971 form; e.g., see *Kieffer* [1985]). The bulk densities of materials at the Viking lander sites, as estimated by *Moore et al.* [1987, p. 126], are consistent with the range assumed by *Neugebauer et al.* [1971]; the bulk density at the Viking 1 lander site is about 1.63 g/cm^3, and at the Viking 2 lander site, the density is about 1.57 g/cm^3. The lighter curves above and below the $\rho c = 0.24$ curve in Figure 2 represent the possible range of volumetric specific heat (ρc) from 0.21 to 0.32 cal °K^{-1} cm^{-3} [*Neugebauer et al.*, 1971]. *Kieffer et al.* [1973] extrapolated the thermal inertia between the known thermal conductivities of 590-840 μm particles and the thermal conductivity of solid basalt; this extrapolation is represented here by dotted curves where $D_p > 10^3$ μm. *Jakosky* [1986] has presented an alternative extrapolation, suggesting that mfp < P_s for grains where $D_p > 10^3$ μm, resulting in a nearly constant thermal inertia of 10 for grains from 10^3 μm to "a few centimeters." We note, however, that there are many surfaces on Mars where $10 < I < I_{(\text{solid rock})}$ [e.g., *Palluconi and Kieffer*, 1981; *Christensen*, 1983; *Zimbelman and Leshin*, 1987] and that pore size (P_s) of 10^3 μm-sized particles is only a factor of 2 greater than mfp at Mars pressures; a leveling off of thermal inertia relative to D_p requires mfp << P_s. Regardless of the manner in which the I and D_p relationship is extrapolated beyond D_p = 10^3 μm, the data presented below for dunes will not require accurate characterization of I for $D_p > 10^3$ μm. Particle sizes given in this paper will be those corresponding to thermal inertias along the solid curve in Figure 2 (where $\rho c = 0.24$), following the precedent of previous workers [e.g., *Neugebauer et al.*, 1971; *Kieffer et al.*, 1973, 1977; *Palluconi and Kieffer*, 1981; *Zimbelman and Leshin*, 1987].

The use of Figure 2 for the interpretation of thermal inertia on Mars comes with several caveats. Figure 2 requires that the surface consist of unconsolidated sediments down to at least a diurnal thermal skin depth (given by $(t\, k\, \rho^{-1}\, c^{-1}\, \pi^{-1})^{0.5}$, where t is time period), which for medium sand on Mars is about 7.5 cm. Figure 2 also assumes that the particles are loosely packed, as packing of unconsolidated sediments may introduce about 15% uncertainty in k [*Fountain and West*, 1970, Figure 4]. Particle shape is also a factor, because nonspherical grains will have increased grain-to-grain surface contacts, thus increasing k [*Wechsler et al.*, 1972]. Finally,

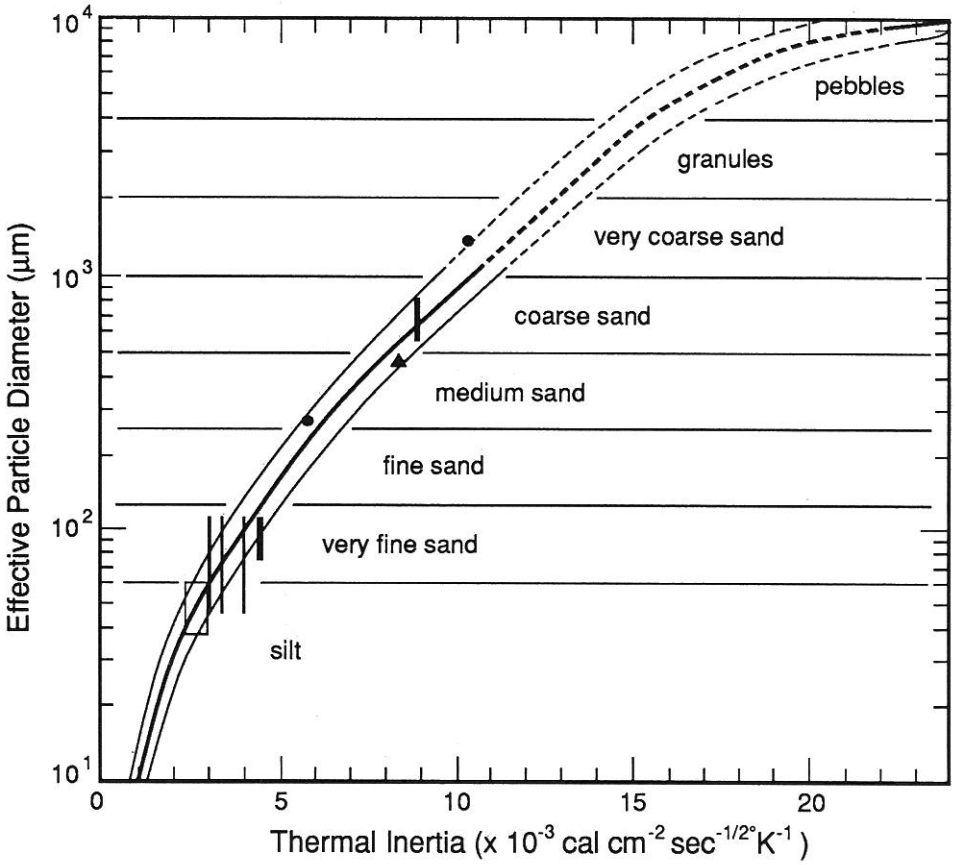

Fig. 2. Thermal inertia as a function of particle size at typical Martian atmospheric pressure and temperature conditions. Vertical bars, box, dots, and triangle represent thermal conductivity data from the literature (assuming $\rho c = 0.24$ cal °K^{-1} cm^{-3}). The heavy curve represents the case where $\rho c = 0.24$ [after *Kieffer et al.*, 1973, Figure 11; *Zimbelman*, 1984, Figure 2.7], the lighter curves represent the thermal inertia for a range of possible ρc (0.21 to 0.32). Curves are dashed where extrapolated beyond 10^3 μm, as discussed by *Kieffer et al.* [1973]. Curves are extrapolated below 40 μm as discussed by *Jakosky* [1986]. Grain sizes are classified according to the *Wentworth* [1922] scale. Data for thin vertical bars are from *Wechsler and Glaser* [1965], thick vertical bars are from *Woodside and Messmer* [1961], box is from *Fountain and West* [1970], triangle is from *Masamune and Smith* [1963], and the dots are from data cited by *Wechsler and Glaser* [1965, Figure 4].

mixtures of particles where pore spaces between larger grains are filled by smaller ones will affect k, such that the particle size estimated from Figure 2 will be an "effective particle size" [*Kieffer et al.*, 1973]. Aeolian dunes present the most ideal material on Mars to avoid these uncertainties. As stated above, dunes consist of a narrow range of grain sizes, thus the "effective particle size" will be very near the actual average grain size. Packing will not be a problem if the dunes are active, which can be determined if they have thermal inertias consistent with unconsolidated materials. Finally, grain shapes will be nearly spherical in a Martian dune, because abrasion and rounding of particles occurs very rapidly under Martian conditions [*Krinsley et al.*, 1979].

Viking IRTM Instrument, Data, and Mars Thermal Models

The Viking IRTM was a scanning radiometer with five midinfrared bands centered on 7, 9, 11, 15, and 20 μm, and one broad, visible and near-IR reflectance band from 0.3 to 3.0 μm [*Chase et al.*, 1978]. The instrument measured the flux of emitted energy from surfaces typically 20-30 km in diameter, or 300-700 km^2; some data collected had higher resolution, generally 2-5 km in diameter or 5-20 km^2.

In this study, two thermal models were used to determine the thermal inertia of dune fields: (1) the "Viking thermal model" of *Kieffer et al.* [1977, Appendix A] and (2) the thermal model of *Haberle and Jakosky* [1991]. The *Kieffer et al.* [1977] model accounts for seasonal and diurnal variations of insolation and conduction into an assumed flat, homogeneous Martian surface (an assumption that should be good for well-sorted materials, like those that occur in dunes). The *Kieffer et al.* [1977] thermal model boundary equation includes terms representing solar insolation, the thermal flux into and out of the surface, and the latent heat of CO_2 (to account for polar frost effects). The *Kieffer et al.* [1977] model assumes that the downward infrared flux in the atmosphere, which includes the effects of solar energy absorption, atmospheric heating, and reradiation by CO_2 and suspended aerosols, can be approximated by assuming that these effects are always 2% of the solar insolation at noon. *Haberle and Jakosky* [1991] found that the atmospheric flux term is usually larger and has a greater diurnal variation than the 2% assumption, resulting in thermal inertias calculated using the *Kieffer et al.* [1977] model that may be higher than the true surface thermal inertia. The *Haberle and Jakosky* [1991] model, however, does not account for the range of seasonal variations incorporated in the *Kieffer et al.* [1977] model, and neither model includes terms for wind advection or the latent heat of H_2O. Elevation effects, not included in the *Kieffer et al.* [1977] model, include the downwelling of infrared radiation as a function of surface atmospheric pressure [*Haberle and Jakosky*, 1991] and pore pressure in particulate surfaces [*Zimbelman*, 1984]. The pressure effects on downwelling IR radiation were incorporated into the *Haberle and Jakosky* [1991]

model, while the pore pressure problem is only significant for the interpretation of thermal inertia at extreme altitudes [*Zimbelman*, 1984].

Haberle and Jakosky [1991] estimated the magnitude of the difference in thermal inertia between their model and the *Kieffer et al.* [1977] model for the Viking 1 lander site (22.5°N) during northern summer. Their results indicated that the *Kieffer et al.* [1977] model overestimates thermal inertia by about 1.7 units when atmospheric dust opacity (τ) is near zero. The difference in the results obtained using the *Kieffer et al.* [1977] model and the *Haberle and Jakosky* [1991] model should, however, vary somewhat with season and latitude. For example, the effects of atmospheric thermal emission to the surface will be reduced in cooler seasons and at higher latitudes. These effects should drop to zero at the poles because of the reduced diurnal temperature range.

Thermal inertia of Martian materials is most effectively determined by establishing the diurnal thermal behavior of the surface. This requires a minimum of two observations of the same surface at different times of the day; these measurements can be fit to a modeled diurnal temperature variation curve and thereby used to fix a reasonable estimate of thermal inertia. For data of high spatial resolution, there are no IRTM observations which were made on the same day or only a few days apart for any single surface location, making it difficult to apply the two-observation analysis. This problem has been solved using a single-point thermal inertia determination [*Kieffer et al.*, 1977, p. 4271; *Palluconi and Kieffer*, 1981]. The reader is referred to a more detailed description of this method by *Christensen* [1983, p. 499]. Basically, the input variables in the single-point method are the 20-μm brightness temperature, latitude, season, and time of day for a given observation, along with an albedo. Daytime observations have a corresponding albedo measurement that can be used as input [*Christensen*, 1983], but nighttime observations require an assumed albedo. *Christensen* [1983] used a constant albedo of 0.25, while *Zimbelman and Leshin* [1987] used 1° by 1° binned IRTM-derived albedos of *Pleskot and Miner* [1981] to study nighttime data. *Christensen* [1983, pp. 499-500] compared results of the single- and dual- point methods and determined that the single-point measurements provide reliable results (65% of compared results were the same to within ±1.5 thermal inertia units), especially during dust-free periods. The single-point method provides the most reliable results when predawn data are used [*Zimbelman and Leshin*, 1987].

The assumption of an albedo (a) in the single-point thermal inertia determination is a potential source of uncertainty. In global thermal inertia mapping projects (which have also used IRTM predawn data), a was assumed to be 0.25 everywhere [*Christensen and Malin*, 1989]. For the dune fields examined in this study, a was assumed to be 0.15. An albedo of 0.15 is a conservative estimate, as many Martian dune fields may have albedos of 0.05-0.13 [*Thomas and Weitz*, 1989]. We found that a difference in albedo of 0.10 results in a difference of thermal inertia, computed by the single-point method, of about 1.0.

Data Selection

The IRTM data used in this study were aquired by both the Viking 1 and 2 orbiters. The data were searched in order to locate the best observations of Martian dune fields. Because the best IRTM data have surface resolutions generally 5-30 km, only large dune fields can be examined. In addition, the dune fields chosen for this study were required to have what appears in Viking or Mariner 9 photographs to be a continuous cover of dune-forming sediment over the field surface. If the interdune surface appeared to be different, as in the case of barchan dunes separated by an interdune surface or a substrate of presumably different thermal inertia, then it was not used (e.g., Figure 3). Large dune fields of generally continuous sediment cover occur in four main regions: the north polar sand sea [*Cutts et al.*, 1976; *Tsoar et al.*, 1979]; the south polar region, especially between latitudes 55°S and 75°S, longitudes 145°W and 250°W [*Thomas*, 1981, 1982]; the Sirenum Terra region, bounded by 55°S to 60°S latitude and 130°W to 145°W longitude [*Peterfreund*, 1985]; and the Hellespontus region (Figures 4 and 5), bounded by latitudes 40°S to 55°S and longitudes 315°W to 350°W [*Cutts and Smith*, 1973; *Breed*, 1977]. An additional large crescentic dune field occurs on the floor of Moreux Crater, located northwest of Syrtis Major at 42.1°N, 315.5°W. While the large dune fields in these regions are assumed here to have a continuous cover of dune-forming sediment, we acknowledge that particle sizes vary throughout any given dune field [*Lancaster*, 1983] and upon any given dune [*Barndorff-Nielsen et al.*, 1982; *Watson*, 1986] and that coarse-grained or cemented/lithified interdune areas might occur in such a dune area [*Sharp*, 1979].

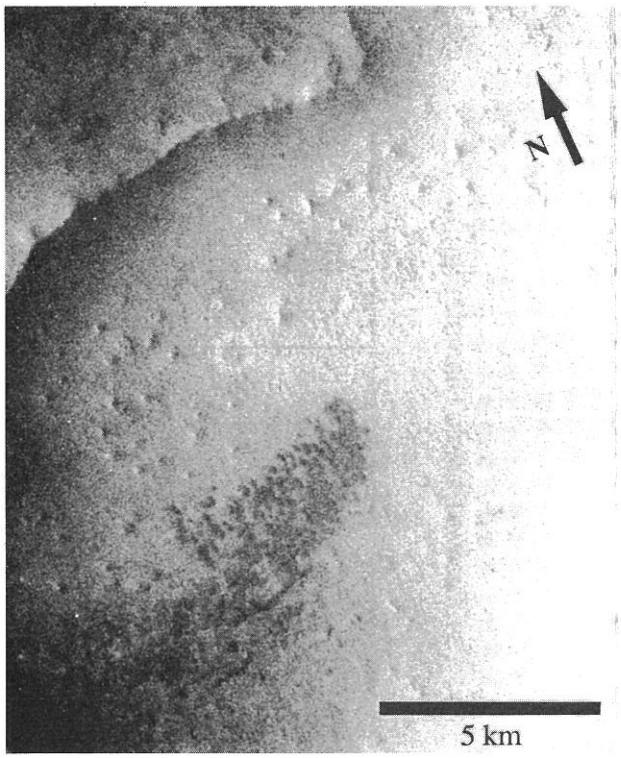

Fig. 3. Small crater in southeastern Oxia Palus containing a dark, barchanoid dune field. Note that the interdune surface is not as dark as the dunes themselves, implying that it is composed of or covered with a different material. (Viking image 709A42, centered near 1.9°N, 351.7°W.)

The IRTM data sought for the thermal inertia investigation were subject to a number of constraints, in order to ensure that the data are the best available. In order to avoid the effects of the major dust storms which occurred during the Viking mission, the data considered here were obtained between Mars heliocentric longitudes (L_s) 344° to 125° [*Ryan and Henry*, 1979; *Christensen*, 1983, 1988]. Data obtained between L_s 344° and 125° correspond to parts of southern summer, autumn, and winter, between October 1977 and August 1978. The data were also constrained by emission angle (0-60°), resolution (2-40 km), and local time of day (21 H to 6 H, where H is 1/24 of the Martian day). The resolution requirement ensures that the IRTM data are only for dune fields which are larger in area than

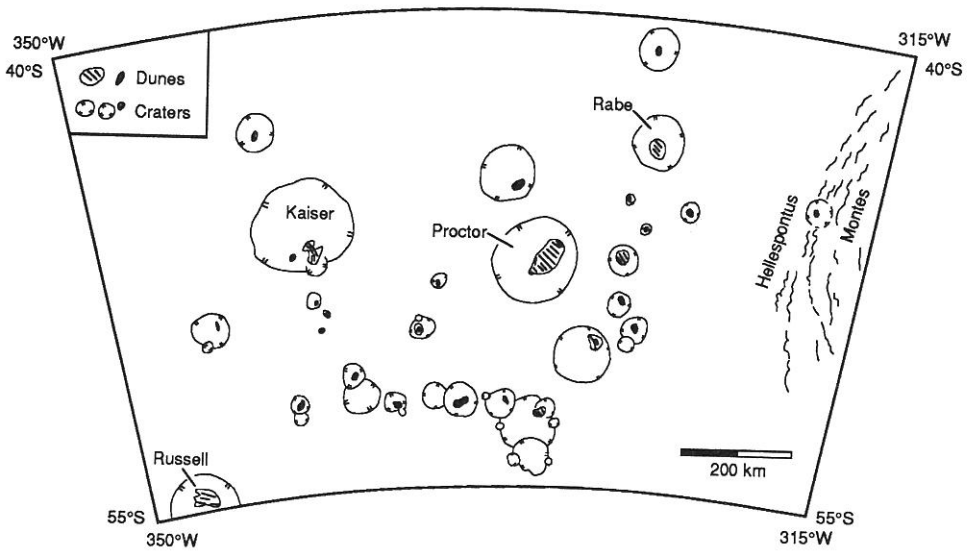

Fig. 4. Sketch map showing the locations of all recognizable dunes in the Hellespontus region of Mars. These dunes include the "Hellespontus Dunes" in Proctor Crater [*Cutts and Smith*, 1973; *Breed*, 1977] photographed by Mariner 9. This sketch shows only those craters which contain known dunes, although many other craters in the region contain dark features. Dune fields represented by parallel lines indicate the dominant strike of dune crests. The following images were used to confirm the presence dunes in the areas indicated: Mariner 9: DAS 8548829; Viking: 93A 47; 94A 33, 42, 45-50; 470A 25; 472A 51; 510A 21, 22, 27-30, 46-48; 547A 43; 581A 09; 358S 21, 23, 24, 26; 94B 49; 575B 8-10, 16, 17, 24, 26, 29, 32, 47, 55, 57-60; 577B 56.

the resolution of the data, so that there is no thermal contribution from surfaces outside the dune field. Careful examination of the latitude and longitude placement of the data also ensure that the data are solely for a dune field. The time-of-day constraint is important in thermal inertia investigations, especially when a single-point inertia is calculated. Data obtained between 21 and 6 H occur at night, when the effects of thermal emission from Sun-heated slopes and the effects of thermal emission due to material composition are minimal, and thermal contrasts due to differences in particle size are at a maximum [e.g., *Kieffer et al.*, 1977; *Palluconi and Kieffer*, 1981]. No data where the brightness temperatures in the 11 μm band were less than in the 20 μm band ($T_{11} - T_{20}$) were used, because negative $T_{11} - T_{20}$ values commonly indicate the presence of water ice clouds which obscure the surface [*Christensen and Zurek*, 1984]. Data were also constrained to avoid surface frosts in the polar regions.

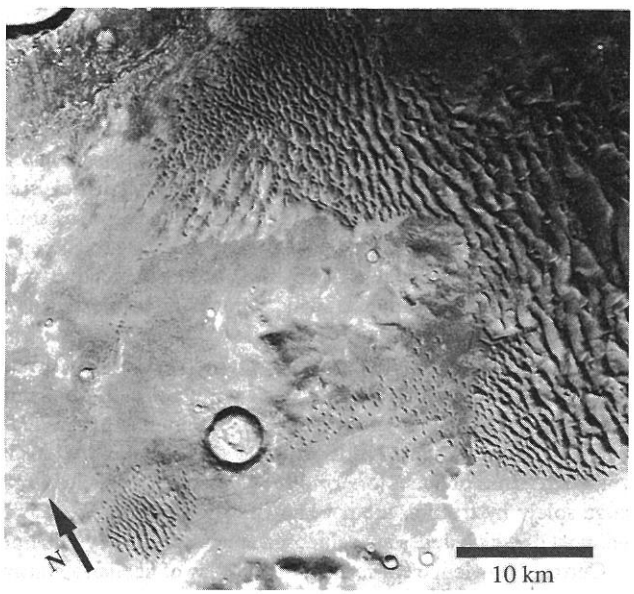

Fig. 5. High-resolution view of the thick, continuous, transverse dune field on the floor of Kaiser Crater. (Viking image 575B60, centered at 47.4°S, 340.5°W.)

Results

IRTM data which meet the above criteria were found for three Martian dune fields which occur on the floors of the Hellespontus craters Kaiser (Figure 5), Rabe, and Proctor. The data, listed in Table 1, are for individual IRTM spots, each one of which is smaller in surface resolution than the dimensions of the dune field. The data for the dune field in Moreux Crater are consistent with those in Hellespontus, although the data spot size exceeds the dimensions of the dune field. However, the dimensions of the dark "splotch" which surrounds and includes the dune field in Moreux Crater is much larger (see Viking orbiter image 269S04) and might also consist of dune-forming sediments.

Thermal inertias were calculated for all of the data using the *Kieffer et al.* [1977] thermal model (Table 1), and all of them are in the range 7.9-8.5, with an average of about 8.2. These thermal inertias assume a surface albedo (a) of 0.15, because the data were obtained at night, when coincident reflectance data are not available. Estimates of albedo for two of the dune fields were obtained by examining daytime IRTM data; a Lambertian albedo of 0.14 was calculated from IRTM reflectance data for the dune field in Kaiser Crater (IRTM sequence 1-504-2-6-947, following the notation in Table 1), and 0.13 for the dunes in Proctor Crater (IRTM sequence 1-509-2-4-1292). If the albedo of the four dune fields in Table 1 is 0.13 instead of 0.15, the calculated thermal inertia would be about 7.9 instead of 8.2. Accounting for the possible uncertainties in the IRTM-derived thermal inertias due to instrument gain and noise (approximately ± 0.25) [e.g., *Kieffer et al.*, 1977; *Pleskot and Miner*, 1981] and the uncertainty in albedo ($a = \pm 0.02$; $I = \pm 0.35$), the maximum uncertainty in the thermal inertia of 8.2 calculated using the *Kieffer et al.* [1977] model is ± 0.6, or about 7%. A thermal inertia

TABLE 1. Thermal Inertia of Intracrater Dunes

Crater Location	Latitude, Longitude	TI[a]	R, km[b]	Dune Field Dimensions, km[c]	Data Identification Numbers				
					S/C[d]	Orbit	Sequence[e]	Spot[f]	Ick[g]
Kaiser	-46.5°, 340.5°	8.1	22.9	50 x 30	1	547	12	6	829
		8.0	23.0		1	547	12	6	830
		8.0	23.3		1	547	12	6	832
Proctor	-47.8°, 330.3°	8.2	27.8	64 x 36	1	545	09	6	762
		8.1	27.3		1	545	09	6	764
Rabe	-43.5°, 325.2°	8.0	22.9	40 x 26	1	545	09	5	640
		7.9	22.8		1	545	09	4	642
		8.5	15.6		1	665	04	4	825
Moreux	42.1°, 315.5°	8.3	32.8	17 x 10	2	523	05	2	323

[a] T I, thermal inertia, assuming albedo of 0.15, calculated using the *Kieffer et al.* [1977] thermal model.

[b] R, resolution, or approximate diameter of the IRTM data spot on the ground, assumed to be approximately circular.

[c] Dune field dimensions, are long and short axis of the approximately elliptical dune fields, measured from Viking images.

[d] S/C, space craft (Viking 1 = 1; Viking 2 = 2).

[e] Sequence, data sequence in the orbit.

[f] Spot, IRTM detector, 1–7 [see *Chase et al.*, 1978, Figure 4].

[g] Ick, number indicating time at which the data were obtained (timed ~1.2 s apart). The spot and ick, taken together, uniquely identify a data point in a sequence.

of 8.2 corresponds to a particle size of about 550 μm (Figure 2), with a possible range, owing to uncertainties in the IRTM instrument properties, in the assumed albedo, and the possible range of ρc, of about 450 to 600 μm, or medium to coarse sand.

The *Haberle and Jakosky* [1991] model was used in an effort to estimate the difference in thermal inertia calculated using their model with respect to the *Kieffer et al.* [1977] model for the Hellespontus dunes (R.M. Haberle, personal communication, 1991). In their work, *Haberle and Jakosky* [1991] determined thermal inertia using an average of 7 and 20 μm brightness temperatures and a dual-observation fit to a diurnal temperature curve. Because of data limitations and a desire for consistency with the usage of the *Kieffer et al.* [1977] model, the *Haberle and Jakosky* [1991] model was applied to our work as a single-point inertia determination from a 20-μm brightness temperature. The following parameters were assumed: $a = 0.15$, $L_s = 20°$, latitude = 48°S, and atmospheric pressure = 610 mbar (corresponding to pressure at the elevation of the Hellespontus dunes, about 1-2 km above datum). The model was run for a low dust opacity ($\tau = 0$) and for what *Haberle and Jakosky* [1991] consider to be a typical dust opacity, appproximately $\tau = 0.4$. It was found that at this latitude and season, atmospheric emission warms the surface on the order of 1°- 3°K on a clear, dust-free day, while a dusty atmosphere ($\tau = 0.37$) would cool the surface by about –5°K. The dust cooling apparently results from the higher solar insolation incidence angles at this latitude and season (this effect results from the scattering of insolation from the suspended dust back into space).

R.M. Haberle (personal communication, 1991) calculated best fit thermal inertias for the Hellespontus dunes of about 7.7 for a clear atmosphere ($\tau = 0$) and about 7.2 for a dusty atmosphere ($\tau = 0.37$). As described above, the maximum uncertainties in thermal inertia due to instrument properties was about ± 0.25, and uncertainty in albedo results in a thermal inertia uncertainty of about ± 0.35. Because only one IRTM observation was used to calculate these results, uncertainty in the derived thermal inertia that is due to the uncertain nature of the diurnal temperature variation is about ±0.2. Thus, the thermal inertias calculated for dunes in Hellespontus using the *Haberle and Jakosky* [1991] model have a maximum uncertainty of about ± 0.8. For a clear atmosphere, the *Haberle and Jakosky* [1991] model gives a thermal inertia of about 7.7 ± 0.8, translating to a particle size of about 470 ± 70 μm. For a dusty atmosphere ($\tau = 0.37$), the thermal inertia is about 7.2 ± 0.8, corresponding to particle sizes of about 400 ± 70 μm.

The *Haberle and Jakosky* [1991] thermal model, therefore, indicates slightly lower thermal inertias for the dunes than those calculated from the *Kieffer et al.* [1977] model. However, the thermal inertias and inferred particle sizes are within the range of uncertainty inherent in the *Kieffer et al.* [1977] model and the assumptions built into the particle size-to-thermal inertia relationship. Most important, both the *Haberle and Jakosky* [1991] model and the *Kieffer et al.* [1977] model indicate that the average particle size of Martian dunes is in the range of 500 ± 100 μm, and is therefore greater than the terrestrial dune average of 250 μm.

3. Particle Sizes at the Transition Between Suspension and Saltation

Review of Aeolian Grain Movement

Particles are moved by the wind in one of three modes: suspension, saltation, or traction (creep). To determine what particle sizes might comprise the dunes on Mars, it is most important to establish what particle sizes may become suspended under Martian conditions. Over time, suspendable particles will be largely removed from a dune (e.g., see observations of wind action upon soils and aeolian drifts by *Daniel* [1936]). Particles that are too big to be lifted by the wind will move as a result of grain impact-induced traction. Under typical terrestrial conditions, particles of granule size (2-4 mm) and larger may move via the creep mechanism. Granule ripples are a common feature in dune fields, especially in hollows and on the windward flanks of dunes [*Sharp*, 1963]. However, particles which move solely by traction are not known to form dunes. The bulk sediment of which dunes are composed are transported by saltation.

Current knowledge concerning the physics of aeolian sediment transport has been obtained through a combination of field observations, wind tunnel experiments, and theoretical modeling. The basic physics was described by *Bagnold* [1941]. *Greeley and Iversen*

[1985] and *Pye and Tsoar* [1990] provided updated reviews of the subject. Here we present a brief summary of material relevant to establishing the particles sizes at the upper limit of suspension (or the lower limit of saltation).

First, consider the case of a spherical particle in the air. Aerodynamic drag tends toward keeping the particle aloft, while the weight of the particle tends to pull it downward. Following the notation of *Greeley and Iversen* [1985], when the drag is equal to the particle weight, the grain has reached its terminal fall velocity,

$$u_f = \left(\frac{4\ \rho_p\, g\ D_p}{3\ \rho_a\, C_d} \right)^{0.5} \tag{1}$$

where D_p is particle diameter, ρ_p is particle density, ρ_a is atmospheric density, g is the acceleration of gravity, and C_d, the drag coefficient, is a function of the Reynolds number, $u\ D_p/\nu$, where ν is the kinematic viscosity ($\nu = \mu/\rho_a$, where μ is absolute viscosity) of the air.

Second, consider a spherical particle at rest in a bed of equal diameter spheres. The forces acting on this particle under windflow conditions are the aerodynamic lift (F_l) and drag (F_d), the particle weight ($F_g = m_p\ g$; m_p is the particle mass), and interparticle forces (F_{ip}), such as electrostatic cohesion [e.g., *Iversen et al.*, 1976*a*]. For the wind to move such a particle, the aerodynamic lift force must overcome the other forces. Interparticle cohesion makes it difficult to move the smallest grains. It follows that for each particle size, there is a threshold drag velocity, u_{*t}, at which the lift forces begin to allow for particle motion.

The drag velocity, u_*, is directly proportional to the rate of increase of the wind velocity with log height above the surface [*Bagnold*, 1941]. In a steady, straight flow, u_* is a measure of the velocity gradient above the bed and is given by

$$u_* = \left(\frac{\tau}{\rho_a} \right)^{0.5} \tag{2}$$

where τ is the fluid shear stress and ρ_a is the fluid density. The surface shear stress at u_{*t} is given by

$$\tau_t = A^2 (\rho_p - \rho_a)\, g\ D_p \tag{3}$$

where A is a dimensionless friction speed,

$$A = u_{*t} \left(\frac{\rho_a}{\rho_p\, g\ D_p} \right)^{0.5} \tag{4}$$

which is a function of the particle friction Reynolds number (B),

$$B = u_{*t} \frac{D_p}{\nu} \tag{5}$$

such that, under terrestrial conditions where $\rho_p >> \rho_a$, A is a function of B and ρ_p/ρ_a. Early investigations of Martian aeolian particle motion also assumed $A = A(B, \rho_p/\rho_a)$, but *Iversen et al.* [1976*a*] and *Greeley et al.* [1980] showed that interparticle cohesion is not linearly proportional to ρ_p, invalidating $A = A(B, \rho_p/\rho_a)$ for Martian conditions.

Iversen and White [1982] derived two empirical expressions useful for determining A under a variety of different planetary conditions:

$$A = 0.129 \left(\frac{\left(\frac{1 + 0.006}{\rho_p\, g\ D_p^{2.5}} \right)^{0.5}}{\left(1.928\ B^{0.092} - 1 \right)^{0.5}} \right) \tag{6}$$

for $0.03 \le B \le 10$, and

$$A = 0.12 \left(\frac{1 + 0.006}{\rho_p\, g\ D_p^{2.5}} \right)^{0.5} \left(1 - 0.0858\ e^{-0.0617\,(B-10)} \right) \tag{7}$$

for $B \ge 10$.

These expressions for A have been used to predict the threshold shear velocity as a function of particle size for Venus, Earth, Mars, Titan, and Triton [*Iversen and White*, 1982; *Greeley and Iversen*, 1985; *Sagan and Chyba*, 1990]. They have also been demonstrated to predict particle motion under experimentally reduced gravity conditions aboard an aircraft [*White et al.*, 1987], and they have been applied to a variety of Martian aeolian topics (review by *Leach et al.* [1989]).

Figure 6 shows the threshold drag velocity as a function of particle size for spheres of density $\rho_p = 2.65$ g/cm^3 for typical terrestrial and Martian conditions, as predicted by *Iversen and White* [1982]. Under terrestrial conditions, the lowest threshold friction velocity needed to initiate particle motion is about 0.22 m/s. The higher threshold friction velocities at lower particle sizes result largely from the cohesive effects of interparticle forces [*Iversen et al.*, 1976*a*]. Large particles also have high threshold friction velocities, due to their greater weight. The threshold friction velocities under Martian conditions are an order of magnitude greater than the terrestrial case, owing to the lower atmospheric pressure and density.

Transition Between Saltation and Suspension

Defining sand as particulate material which is movable either by direct pressure of the wind or by impact-induced motion, *Bagnold* [1941, pp. 6 and 98] defined the lower limit of sand (or the upper limit of suspendable material) "as that at which the terminal velocity of fall

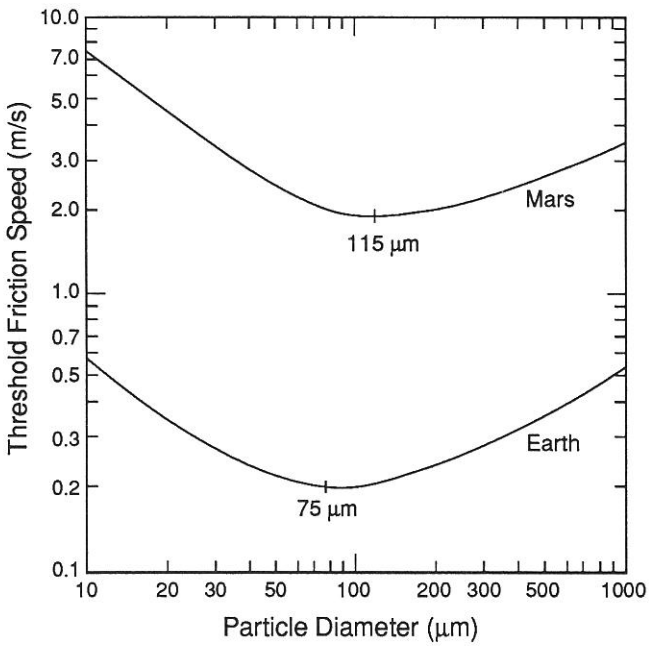

Fig. 6. Approximate average threshold friction speed comparisons for Earth and Mars, as given by equations (6) and (7). Particle densities (ρ_p) for both are 2.65 g/cm^3. Martian atmospheric density (ρ_M) is 1.10 x 10^{-5} g/cm^3, terrestrial atmospheric density (ρ_E) is 1.23 x 10^{-3} g/cm^3, Mars atmosphere kinematic viscosity (ν_M) is 11.19 cm^2/s, Earth atmosphere kinematic viscosity (ν_E) is 0.146 cm^2/s, Mars gravitational acceleration (g_M) is 375 cm/s^2, and Earth gravitational acceleration (g_E) is 981 cm/s^2. The optimum particle sizes (75 μm for Earth and 115 μm for Mars) are indicated. (Modified after *Iversen and White* [1982] with permission from Blackwell Scientific Publications.)

becomes less than the upward eddy currents within the average surface wind." The transition from suspension to saltation of aeolian particles is not distinct. Pure saltation occurs when the vertical fluctuating component of wind velocity (w') has no significant effect on the particle trajectory, while pure suspension occurs when the particle settling velocity (u_f) is small with respect to the surface wind friction velocity (u_*) [e.g., *Nalpanis,* 1985]. *Tsoar and Pye* [1987, p. 141] explain that the force which opposes the tendency for small particles to remain aloft (in a neutrally stratified atmosphere near the surface) is the standard deviation of the mean vertical fluctuating component of wind velocity, W'. If the standard deviation of W' is greater than the settling velocity (u_f), then the particle will remain suspended. The standard deviation of W' is equal to a constant, R, times the velocity gradient, u_*. The value of R is the ratio, u_f/u_*, which is commonly taken as an approximation of the conditions which determine whether a particle can become suspended in a fluid [e.g., *Bagnold,* 1941; *Middleton,* 1976; *Tsoar and Pye,* 1987]. The arbitrary boundary between suspension and saltation occurs where $u_f/u_* = 1$ [*Tsoar and Pye,* 1987]. *Gillette et al.* [1974] established an upper limit for pure suspension at approximately $u_f/u_* = 0.7$, and the values $0.7 \leq u_f/u_* \leq 2.5$ are generally considered a zone of "modified saltation," where air turbulence has a significant effect on the paths of airborne particles [*Nalpanis,* 1985; *Hunt and Nalpanis,* 1985]. In general, particles are in pure saltation if $u_f/u_* >> 2.5$ and in pure suspension if $u_f/u_* \leq 0.7$ [*Tsoar and Pye,* 1987; *Anderson,* 1987].

Figure 7 shows the ratio of terminal fall velocity, u_f, to threshold friction velocity, u_{*t}, for spherical particles modeled under the same conditions as in Figure 6 for terrestrial and Martian cases [from *Greeley and Iversen,* 1985]. Figure 7 indicates that particles ≤ 52 μm go directly into suspension when the threshold friction velocity occurs [*Iversen et al.,* 1976*b*; *Greeley and Iversen,* 1985, pp. 70 and 95]. In fact, particles in the range 40-80 μm may undergo modified saltation [*Nalpanis,* 1985], and nearly all grains in terrestrial dunes are more coarse than 52 μm [*Ahlbrandt,* 1979; *Greeley and Iversen,* 1985]. Even in the finest terrestrial windblown sands, the average diameter is seldom less than about 80 μm [*Bagnold,* 1941, p. 6].

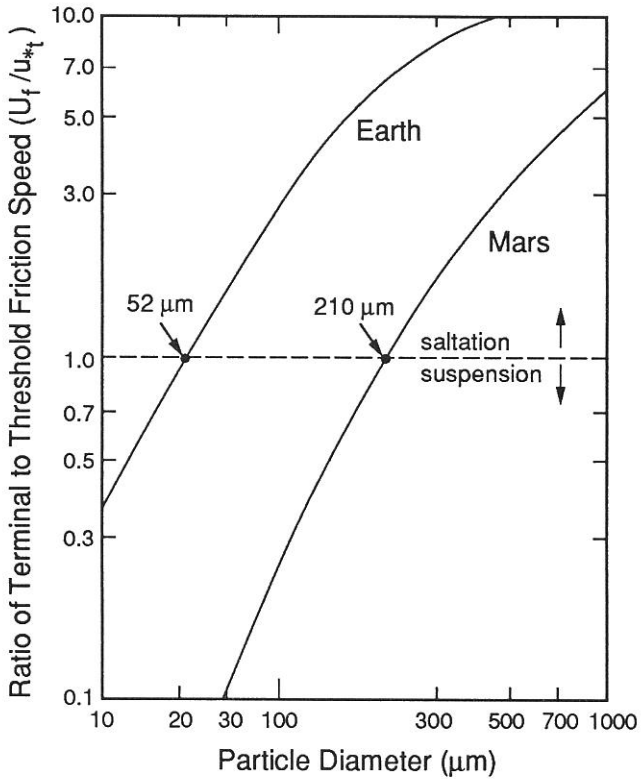

Fig. 7. Ratio of the terminal velocity (u_f) to threshold friction velocity (u_{*t}) for the Earth and Mars as a function of particle size. The physical properties of the particles, atmosphere, and gravitational acceleration are the same as in Figure 6. The approximate saltation-suspension boundary occurs when u_f/u_{*t} = 1.0. For Earth, this ratio is 1.0 for particles ~ 52 μm in size, for Mars, 210 μm. (Modified after *Greeley and Iversen* [1985, Figure 3.2] with permission from Cambridge University Press.)

Suspension of Particles on Mars

Martian atmospheric pressures and temperatures vary with elevation, time of day, and season [e.g., *Pollack et al.,* 1981; *Hess et al.,* 1977]. However, aeolian activity has been observed from the lowest elevations (Hellas Basin floor) [*Briggs et al.,* 1979; *Peterfreund,* 1985] to the highest volcano summits [*Sagan et al.,* 1974; *Lee et al.,* 1982; *Lee,* 1986]. Surface atmospheric pressures range from as high as 15 mbar in low regions to 1 mbar at the highest elevations. Changes in pressure and temperature affect the density (ρ_a) and kinematic viscosity (ν) of the Martian atmosphere. Large differences in atmospheric properties alter the properties of the wind surface shear [*Greeley et al.,* 1980], thus changing the characteristics of aeolian particle entrainment and motion [*White,* 1979, p. 4646]. When the atmospheric pressure is at its highest and the temperature is at its lowest (resulting in the highest possible ρ_a), equations (6) and (7) predict a minimal threshold friction velocity, u_{*t}, of ~ 1 m/s [*Iversen and White,* 1982]. The typical minimum Martian u_{*t} is near 2 m/s.

Figure 7 shows that $u_f/u_* = 1$ for general Martian conditions when the particle size is about 210 μm, suggesting that particles ≤ 210 μm are typically susceptible to suspension [*Iversen et al.,* 1976*b*; *Greeley and Iversen,* 1985]. Slight differences in which particle sizes may saltate or go into suspension, however, likely occur at different elevations or latitudes, depending on variations in atmospheric pressure and temperature [*White,* 1979]. *Greeley and Iversen* [1985, p. 70] suggested on the basis of this diagram (Figure 7) that Martian dunes should have few grains smaller than 210 μm, and therefore Martian dunes may be coarser than dunes on Earth.

It may seem counterintuitive that particles as large as 210 μm could become suspended in the thin Martian atmosphere, especially considering that on Earth the particles at the $u_f/u_* = 1$ boundary are 4 times smaller. However, two main factors act together to cause large particles to become suspended: (1) the high surface friction velocity (u_*) needed to move particles at the low Martian atmospheric pressures; and (2) the lower gravity of Mars (375 cm/s^2). The higher particle velocity and lower gravity, in combination with a reduced atmospheric drag in the thin Martian air, create longer path lengths for saltating particles [*White et al.,* 1976; *White,* 1979]. As saltation path length approaches infinity, it becomes more likely that a particle will be suspended [*Anderson,* 1987, p. 508]. (Note that the opposite effect occurs on Venus, where u_{*t} values are an order of magnitude less than on Earth, and the dense atmosphere creates a strong drag on windborne particles, giving them shorter path lengths than might occur on Earth and Mars [*Iversen et al.,* 1976*a*; *White,* 1981; *Iversen and White,* 1982; *Greeley et al.,* 1984].)

Saltation Path Length on Earth and Mars

Another way to examine the question of Martian dune particle size is to compare saltation path length as a function of particle size for Martian and terrestrial conditions. At small, suspendable particle sizes, the path length should approach infinity. At the particle sizes which are in the size range that can saltate under given planetary

conditions, the path length should not vary as strongly as grains which can be suspended. For this discussion of particle trajectory path length (defined as the distance along the ground over which the particle travels) as a function of particle size, we present a comparison between Earth and Mars cases.

The saltation trajectory of a grain is calculated by solving for y and u_p as a function of x (where x is horizontal distance, y is vertical distance, u_p is velocity of particle relative to air) over the particle trajectory. The acceleration of the particle is given by

$$a_p = g + F_d - (F_l + F_m) \tag{8}$$

where the forces refer to gravity (g), aerodynamic drag (F_d) and lift (F_l), and Magnus (spin) forces (F_m). Lift forces are only important at the begining of grain movement; for our purposes they can be simulated by modifying ω_0, the liftoff velocity of the particle. Magnus forces [*White and Schultz*, 1977] can be ignored in this example. Following *Bagnold* [1941] and *Anderson* [1987], the drag force is given by

$$F_d = \frac{1}{2} C_d P_a \rho_a u_p^2 \tag{9}$$

in which P_a is the cross-sectional area of the particle ($\pi D_p^2/4$ for a sphere). The acceleration of the particle during its motion through the air, without lift forces, is given by

$$a_p = \frac{3 C_d \rho_a u_p^2}{4 \rho_p D_p} + g \tag{10}$$

where the drag coefficient is a function of the Reynolds number as given by the curve-fitting formulae listed by *Morsi and Alexander* [1972, p. 207].

To calculate trajectory as a function of particle size, an initial particle ejection velocity, ω_0, is used. This velocity may be either the lift-off velocity of particles initially at rest and suddenly exposed to winds at u_{*t}, or the velocity imparted by other, impacting grains. *Bagnold* [1941] assumed that ω_0 is proportional to the drag velocity, in this case u_{*t}, such that $\omega_0 = \alpha u_{*t}$; this relationship is commonly used to estimate ω_0 by assuming a reasonable value for α. For particles where the entire bed is initially at rest, the effects of lift forces (F_l and F_m) can be simulated by assuming that α is a function of particle size [*White et al.*, 1975, 1976]. For particles in an already active environment, where all ejection is due to the impact of other grains, ω_0 can be considered a constant [*Bagnold*, 1941, chapter 5]. *Bagnold* [1941] found α to be about 0.8 for such grains under terrestrial conditions.

Figure 8 shows two diagrams of saltation path length as a function of particle size for grains at their threshold friction velocity ($u_{*t}(D_p)$) under terrestrial and Martian conditions (u_{*t} from *Iversen and White* [1982]). In both diagrams, the particle trajectories were calculated for spherical grains with a density, $\rho_p = 2.65$ g/cm^3, under the same atmospheric conditions as used by *Iversen and White* [1982]. The algorithms used to calculate path length were compared with the work of *White et al.* [1976] and *White* [1979], and were found to be consistent with White's results for no-lift forces cases. In Figure 8*a*, α was assumed to be a function of particle size, in order to simulate grain motion in an initially immobile bed (where lift forces are important). The values for α used in Figure 8*a* come from *White et al.* [1975, Figure 36] for Earth and *White et al.* [1976, Figure 9] for Mars. In Figure 8*b*, α was assumed to be constant for all particle sizes, as might be the case where particle motion is induced by the impact of other grains [*Bagnold*, 1941]. For the Martian case, α is assumed to be 0.1 [after *White*, 1979], and for Earth, it is assumed to be 1.0 (which is close to Bagnold's $\alpha = 0.8$). It can be seen, in both Figures 8*a* and 8*b*, that at smaller particle sizes the path length asymptotically approaches infinity, indicating, as expected, that decreasing particle sizes are increasingly susceptible to suspension. The longer the path length, the more likely it is to be kept aloft by turbulence and removed from a saltating, granular surface [e.g., *Anderson*, 1987].

In both Figures 8*a* and 8*b*, the "zone" of modified saltation ($0.7 \le u_f/u_* \le 2.5$) and the particle size where $u_f/u_{*t} = 1.0$ from Figure 7 are shown. The zone of modified saltation corresponds approximately to the inflection portion of the curves, especially in Figure 8*b*. What is most important about both of these diagrams is the difference between the inflection points for Mars and Earth. This is especially apparent in Figure 8*b*, where the curve for Earth turns over at particles sizes of about 50-80 μm, while the Mars curve turns over at about 200-250 μm, a difference of 150-170 μm. This diagram supports both our thermal inertia results and the contention of *Greeley and Iversen* [1985, p. 70], which indicate that Martian dunes are more coarse grained than terrestrial dunes.

4. Discussion

Most of the sediment in terrestrial dunes are grains coarser than 52 μm (where $u_f/u_{*t} = 1$), and terrestrial dune sands have a mean value (~250 μm) in the fine to medium sand range [e.g., *Bagnold*, 1941; *Ahlbrandt*, 1979]. Because of the difference between the terrestrial particle size where $u_f/u_{*t} = 1$ (52 μm) and the Martian particle size where $u_f/u_{*t} = 1$ (210 μm), *Greeley and Iversen* [1985, p. 70] suggested that Martian dune sands should, on average, be composed of particles larger than in terrestrial dunes. In this study, we have demonstrated the idea of *Greeley and Iversen* [1985] in Figure 8, which shows that larger particles, up to ~210 μm, should indeed have longer path lengths on Mars than on Earth, due to the reduced gravity, greater u_{*t}, and reduced atmospheric drag. In addition, we have presented well-constrained IRTM thermal-infrared data for three Martian dune areas in the Hellespontus region. Both of the thermal models presented above give thermal inertias in the range of 7.2-8.5 with uncertainties of ± 0.6 to 0.8, indicating effective particle sizes of about 500 ± 100 μm. Though both approaches explored here, thermal inertia and saltation physics, are model-dependent, these models make independent assumptions and are based upon several decades of research. Both methods indicate that the Martian dunes should be coarser grained than terrestrial dunes.

As indicated above, there are no other dune areas large enough to have been studied by IRTM data which met the other constraint criteria. However, *Keegan et al.* [1991] have presented results of carefully modeled, IRTM-derived thermal inertia figures for the north polar region. They found that many of the large, continuous dune fields of the north polar erg have thermal inertias in the range 7.5-10, a result consistent with the findings presented in this paper. The estimated average Martian dune particle size can be applied to further our understanding of other sandy areas on Mars. There are a number of places on Mars where active sand is a probable component of the surface. Such areas are those where there is both a low rock abundance and the fine component thermal inertia is in the range 7-10 [*Christensen*, 1986]. Many low albedo, intracrater dark features, or "splotches," have thermal inertias in the 7-10 range [*Christensen*, 1983], and most may be sandy areas [*Arvidson*, 1974; *Christensen*, 1983; *Thomas*, 1984]. Other dark, probably sandy regions include the Meridiani Sinus region [*Presley and Arvidson*, 1988], and Syrtis Major, which has dunes [*Peterfreund*, 1981; *Simpson et al.*, 1982] as well as a low rock abundance coupled with fine component thermal inertias in the range 7-9 [*Christensen*, 1986].

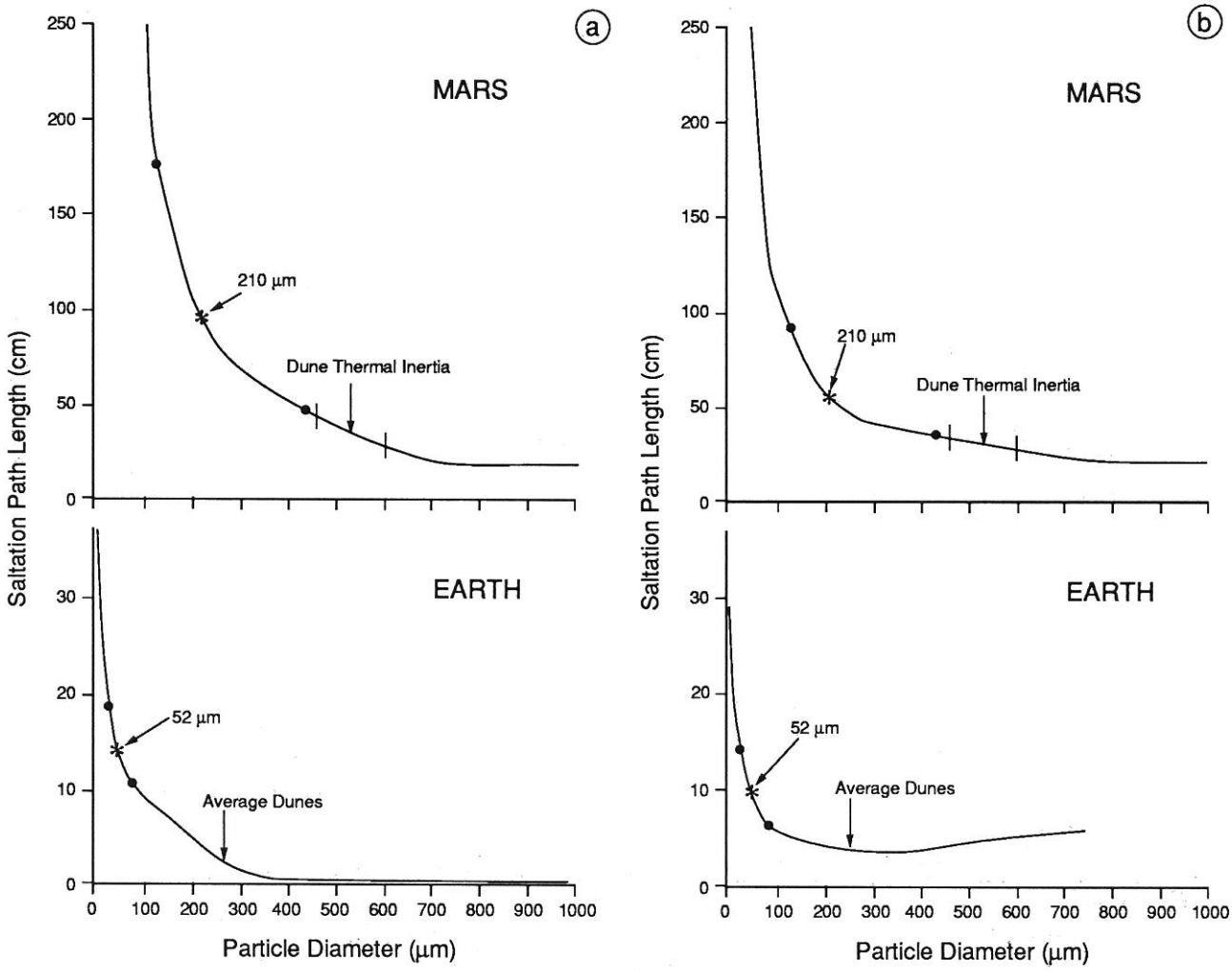

Fig. 8. Saltation path length as a function of particle size for spherical particles where $\rho_p = 2.65$ g/cm^3. The physical properties of the atmosphere (ν, ρ_a) and gravitational acceleration (g) are the same as in Figures 6 and 7. The roughness height, z_0, was assumed to be 1/30 D_p [*Bagnold*, 1941, p. 99]. Lift-off or ejection velocities (ω_0) were assumed to be proportional to u_{*t}, such that $\omega_0 = \alpha u_{*t}$. *(a)* α is given as a function of particle size, in order to simulate lift-off velocities for grains in a bed initially at rest, using α derived from *White et al.* [1975, Figure 36] for Earth and *White et al.* [1976, Figure 9] for Mars. *(b)* α is given as a constant, simulating average conditions when ejection results from grain impacts [*Bagnold*, 1941], such that for Mars, $\alpha = 0.1$ and for Earth, $\alpha = 1.0$. In both Figures 8*a* and 8*b*, the particle size where $u_{*f}/u_{*t} = 1$ for Earth (52 μm) and Mars (210 μm) are labeled with asterisks and the range of "modified saltation" is indicated by small solid circles. The particle size and probable uncertainty of the thermal inertia results for Martian dunes are indicated by an arrow and two vertical bars. Note the difference in vertical axis scale for the Earth and Mars cases.

5. Summary

Two independent approaches indicate that Martian aeolian dunes have a particle size that is greater than the terrestrial average. On Earth, the average dune grains are about 250 μm, or fine to medium sand. Thermal inertias, calculated from Viking IRTM mid-IR emission data using both the *Kieffer et al.* [1977] and *Haberle and Jakosky* [1991] thermal models, indicate that Martian dunes have thermal inertias near 8.0, corresponding to unimodal particle sizes in the medium to coarse sand range, with average particle sizes of about 500 ± 100 μm. Because dunes are composed entirely of materials which move by saltation or traction, grains which can become suspended will not be found in an active dune. The largest particle that can become suspended under terrestrial conditions is about 52 μm, and nearly all dune sand is coarser than this size. On Mars, particles of about 210 μm may be susceptible to suspension, and pure saltation occurs at particle sizes > 430 μm (at which $u_f/u_{*t} \approx 2.5$). These results suggest that Martian dunes will consist entirely of sand coarser than 210 μm, and the mean is probably larger than 430 μm. Particle trajectory path lengths are greater under Martian conditions, owing to reduced gravity, reduced atmospheric drag, and the higher surface friction velocities required to move grains on Mars; suggesting, again, that coarser particles can saltate and form dunes on Mars. The combined examination of independent models, saltation physics and thermal inertia modeling, indicate (1) that Martian dunes are coarser grained than terrestrial dunes, and (2) that the relationship between thermal inertia and particle size (which has been used in the past to study the distribution of surface grain sizes on Mars) is generally valid.

Acknowledgments. We are grateful to R.M. Haberle, who calculated thermal inertias for the dunes using the Haberle and Jakosky (1991) thermal model. Prompt reviews and thoughtful comments from B.M. Jakosky and J.D. Iversen were much appreciated. R. Greeley provided additional helpful comments on the manuscript. Discussions with M.C. Malin, N. Lancaster, D. Krinsley, and M.A. Presley also proved instructive. S. Selkirk was

instrumental in preparing the figures, and D. Ball assisted with the photographs. D. Aitkin helped typeset the document. This research is supported by NASA grants NAGW 2289 and NAGW 943.

REFERENCES

Ahlbrandt, T.S., Textural parameters of eolian deposits, in A Study of Global Sand Seas, edited by E.D. McKee, *U.S. Geol. Surv. Prof. Pap., 1052*, 21-51, 1979.

Anderson, R.S., Eolian sediment transport as a stochastic process: The effects of a fluctuating wind on particle trajectories, *J. Geol., 95*, 497-512, 1987.

Arvidson, R.E., Wind-blown streaks, splotches, and associated craters on Mars: Statistical analysis of Mariner 9 photographs, *Icarus, 21*, 12-27, 1974.

Bagnold, R.A., *The Physics of Blown Sand and Desert Dunes*, 265 pp., Methuen, London, 1941.

Barndorff-Nielsen, O., K. Dalsgaard, C. Halgreen, H. Kuhlman, J.T. Moller, and G. Schon, Variation in particle size over a small dune, *Sedimentology, 29*, 53-65, 1982.

Breed, C.S., Terrestrial analogs of the Hellespontus dunes, Mars, *Icarus, 30*, 326-340, 1977.

Breed, C.S., M.J. Grolier, and J.F. McCauley, Morphology and distribution of common 'sand' dunes on Mars: Comparison with the Earth, *J. Geophys. Res., 84*, 8183-8204, 1979.

Briggs, G.A., W.A. Baum, and J. Barnes, Viking orbiter observations of dust in the Martian atmosphere, *J. Geophys. Res., 84*, 2795-2820, 1979.

Chase, S.C. Jr., J.L. Engel, H.W. Eyerly, H.H. Kieffer, F.D. Palluconi, and D. Schofield, Viking infrared thermal mapper, *Appl. Opt., 17*, 1243-1251, 1978.

Chepil, W.S., and N.P. Woodruff, The physics of wind erosion and its control, *Adv. Agron., 15*, 211-302, 1963.

Christensen, P.R., Eolian intracrater deposits on Mars: Physical properties and global distribution, *Icarus, 56*, 496-518, 1983.

Christensen, P.R., The spatial distribution of rocks on Mars, *Icarus, 68*, 217-238, 1986.

Christensen, P.R., Global albedo variations on Mars: Implications for active aeolian transport, deposition, and erosion, *J. Geophys. Res., 93*, 7611-7624, 1988.

Christensen, P.R., and M.C. Malin, High-resolution thermal imaging of Mars, in Planetary Geosciences-1988, edited by M. Zuber, O. James, G. MacPherson, and J. Plescia, *NASA Spec. Publ., SP-498*, 6-7, 1989.

Christensen, P.R., and R.W. Zurek, Martian north polar hazes and surface ice: Results from the Viking Survey/Completion Mission, *J. Geophys. Res., 89*, 4587-4596, 1984.

Cutts, J.A., and R.S.U. Smith, Eolian deposits and dunes on Mars, *J. Geophys. Res., 78*, 4139-4154, 1973.

Cutts, J.A., K.R. Blasius, G.A. Briggs, M.H. Carr, R. Greeley, and H. Masursky, North polar region of Mars: Imaging results from Viking 2, *Science, 194*, 1329-1337, 1976.

Daniel, H.A., The physical changes in soils of the southern high plains due to cropping and wind erosion and the relation between the (sand + silt)/clay ratios in these soils, *J. Am. Soc. Agron., 28*, 570-580, 1936.

Fountain, J.A., and E.A. West, Thermal conductivity of particulate basalt as a function of density in simulated lunar and Martian environments, *J. Geophys. Res., 75*, 4063-4069, 1970.

Gillette, D.A., I.H. Blifford Jr., and D.W. Fryrear, The influence of wind on the size distribution of aerosols generated by the wind erosion of soils, *J. Geophys. Res., 79*, 4068-4075, 1974.

Greeley, R., and J.D. Iversen, *Wind as a Geological Process on Earth, Mars, Venus, and Titan*, 333 pp., Cambridge University Press, New York, 1985.

Greeley, R., R. Leach, B. White, J. Iversen, and J. Pollack, Threshold windspeeds for sand on Mars: Wind tunnel simulations, *Geophys. Res. Lett., 7*, 121-124, 1980.

Greeley, R., J. Iversen, R. Leach, J. Marshall, B. White, and S. Williams, Windblown sand on Venus: Preliminary results of laboratory simulations, *Icarus, 57*, 112-124, 1984.

Haberle, R.M., and B.M. Jakosky, Atmospheric effects on the remote determination of thermal inertia on Mars, *Icarus, 90*, 187-204, 1991.

Hess, S.L., R.M. Henry, C.B. Leovy, J.A. Ryan, and J.E. Tillman, Meteorological results from the surface of Mars: Viking 1 and 2, *J. Geophys. Res., 82*, 4559-4574, 1977.

Hunt, J.C.R., and P. Nalpanis, Saltating and suspended particles over flat and sloping surfaces, I. Modelling concepts, in *Proceedings of the International Workshop on the Physics of Blown Sand, Mem. 8*, edited by O.E. Barndorff-Nielsen et al., pp. 9-36, Department of Theoretical Statistics, Institute Mathematics, University of Aarhus, Denmark, 1985.

Iversen, J.D., and B.R. White, Saltation threshold on Earth, Mars, and Venus, *Sedimentology*, 29, 111-119, 1982.

Iversen, J.D., J.B. Pollack, R. Greeley, and B.R. White, Saltation threshold on Mars: The effect of interparticle force, surface roughness, and low atmospheric density, *Icarus, 29*, 381-393, 1976*a*.

Iversen, J.D., R. Greeley, and J.B. Pollack, Windblown dust on Earth, Mars, and Venus, *J. Atmos. Sci., 33*, 2425-2429, 1976*b*.

Jakosky, B.M., On the thermal properties of Martian fines, *Icarus, 66*, 117-124, 1986.

Keegan, K.D., J.E. Bachman, and D.A. Paige, Thermal and albedo mapping of the north polar region of Mars (abstract), *Lunar Planet. Sci., XXII*, 701-702, 1991.

Kieffer, H.H., S.C. Chase Jr., E. Miner, G. Münch, and G. Neugebauer, Preliminary report on infrared radiometric measurements from the Mariner 9 spacecraft, *J. Geophys. Res., 78*, 4291-4312, 1973.

Kieffer, H.H., T.Z. Martin, A.R. Peterfreund, B.M. Jakosky, E.D. Miner, and F.D. Palluconi, Thermal and albedo mapping of Mars during the Viking primary mission, *J. Geophys. Res., 82*, 4249-4292, 1977.

Kieffer, S.W., Heat capacity and entropy: Systematic relations to lattice vibrations, *Rev. Mineral., 14*, 65-126, 1985.

Krinsley, D., R. Greeley, and J.B. Pollack, Abrasion of windblown particles on Mars- Erosion of quartz and basaltic sand under simulated Martian conditions, *Icarus, 39*, 364-384, 1979.

Lancaster, N., Controls of dune morphology in the Namib sand sea, *Dev. Sedimentol., 38*, 261-289, 1983.

Leach, R., R. Greeley, and J. Pollack, Saltation thresholds and entrainment of fine particles at Earth and Martian pressures, *NASA Tech. Memo., TM-102193*, 38 pp., 1989.

Lee, S.W., Dust transport at high altitudes and low pressures on Mars: Aeolian activity on the Tharsis Montes (abstract), Reports of Planetary Geology and Geophysics Program-1985, *NASA Tech. Memo, TM-88383*, 251-253, 1986.

Lee, S.W., P.C. Thomas, and J. Veverka, Wind streaks in Tharsis and Elysium: Implications for sediment transport by slope winds, *J. Geophys. Res., 87*, 10,025-10,041, 1982.

Liu, N.C., and W.I. Dobar, The nature of the lunar surface: The thermal conductivity of dust and pumice, in *The Lunar Surface Layer, Materials and Characteristics*, edited by J.W. Salisbury and P.E. Glaser, pp. 381-387, Academic, New York, 1964.

Masamune, S., and J.M. Smith, Thermal conductivity of beds of spherical particles, *Ind. Eng. Chem. Fundam., 2*, 136-143, 1963.

Middleton, G.V., Hydraulic interpretation of sand size distributions, *J. Geol., 84*, 405-426, 1976.

Moore, H.J., R.E. Hutton, G.D. Clow, and C.D. Spitzer, Physical properties of the surface materials at the Viking landing sites on Mars, *U.S. Geol. Surv. Prof. Pap., 1389*, 222 pp., 1987.

Morsi, S.A., and A.J. Alexander, An investigation of particle trajectories in two-phase flow systems, *J. Fluid Mech., 55*, 193-208, 1972.

Muhleman, D.O., Microwave emission from the Moon, in Thermal Characteristics of the Moon, edited by J.W. Lucas, *Prog. Astronaut. Aeronaut., 28*, 51-81, 1972.

Nalpanis, P., Saltating and suspended particles over flat and sloping surfaces II. Experiments and numerical simulations, in *Proceedings of the International Workshop on the Physics of Blown Sand, Mem. 8*, edited by O.E. Barndorff-Nielsen et al., pp. 37-66, Department of Theoretical Statistics, Institute of Mathematics, University of Aarhus, Denmark, 1985.

Neugebauer, G., G. Münch, H. Kieffer, S.C. Chase Jr., and E. Miner, Mariner 1969 infrared radiometer results: Temperatures and thermal properties of the Martian surface, *Astron. J., 76*, 719-728, 1971.

Palluconi, F.D., and H.H. Kieffer, Thermal inertia mapping of Mars from 60°S to 60°N, *Icarus, 45*, 415-426, 1981.

Peterfreund, A.R., Visual and infrared observations of wind streaks on Mars, *Icarus, 45*, 447-467, 1981.

Peterfreund, A.R., Contemporary aeolian processes on Mars: Local dust storms, Ph.D. dissertation, 246 pp., Ariz. State Univ., Tempe, 1985.

Peterfreund, A.R., R. Greeley, and D. Krinsley, Martian sediments: Evidence for sand on Mars (abstract), Reports of Planetary Geology Program-1981, *NASA Tech. Memo., TM-84211*, 205-207, 1981.

Pleskot, L.K., and E.D. Miner, Time variability of Martian bolometric albedo, *Icarus, 45*, 179-201, 1981.

Pollack, J.B., C.B. Leovy, P.W. Greiman, and Y. Mintz, A Martian general circulation experiment with large topography, *J. Atmos. Sci., 38*, 3-29, 1981.

Presley, M.A., and R.E. Arvidson, Nature and origin of materials exposed in

the Oxia Palus-Western Arabia-Sinus Meridiani Region, Mars, *Icarus*, *75*, 499-517, 1988.
Pye, K., and H. Tsoar, *Aeolian Sand and Sand Dunes*, 396 pp., Unwin Hyman, London, 1990.
Ryan, J.A., and R.M. Henry, Mars atmospheric phenomena during major dust storms as measured at the surface, *J. Geophys. Res.*, *84*, 2821-2829, 1979.
Sagan, C., and C. Chyba, Triton's streaks as windblown dust, *Nature*, *346*, 546-548, 1990.
Sagan, C., J. Veverka, R. Steinbacher, L. Quam, R. Tucker, and B. Eross, Variable features on Mars, IV, Pavonis Mons, *Icarus*, *22*, 24-47, 1974.
Sharp, R.P., Wind ripples, *J. Geol.*, *71*, 617-636, 1963.
Sharp, R.P., Intradune flats of the Algodones chain, Imperial Valley, California, *Geol. Soc. Am. Bull.*, *90*, 908-916, 1979.
Simpson, R.A., G.L. Tyler, J.K. Harmon, and A.R. Peterfreund, Radar measurement of small-scale surface texture: Syrtis Major, *Icarus*, *49*, 258-283, 1982.
Thomas, P., North-south asymmetry of eolian features in Martian polar regions: Analysis based on crater-related wind markers, *Icarus*, *48*, 76-90, 1981.
Thomas, P., Present wind activity on Mars: Relation to large latitudinally zoned sediment deposits, *J. Geophys. Res.*, *87*, 9999-10,008, 1982.
Thomas, P., Martian intracrater splotches: Occurrence, morphology, and colors, *Icarus*, *57*, 205-227, 1984.
Thomas, P., and C. Weitz, Sand dune materials and polar layered deposits on Mars, *Icarus*, *81*, 185-215, 1989.
Tsoar, H., and K. Pye, Dust transport and the question of desert loess formation, *Sedimentology*, *34*, 139-153, 1987.
Tsoar, H., R. Greeley, and A.R. Peterfreund, Mars: The North Polar Sand Sea and related wind patterns, *J. Geophys. Res.*, *84*, 8167-8180, 1979.
Watson, A., Grain size variations on a longitudinal dune and a barchan dune, *Sediment. Geol.*, *46*, 49-66, 1986.
Wechsler, A.E., and P.E. Glaser, Pressure effects on postulated lunar materials, *Icarus*, *4*, 335-352, 1965.
Wechsler, A.E., P.E. Glaser, and J.A. Fountian, Thermal properties of granulated materials, in Thermal Characteristics of the Moon, edited by J.W. Lucas, *Prog. Astronaut. Aeronaut.*, *28*, 215-241, 1972.
Wentworth, C.K., A scale of grade and class terms for clastic sediments, *J. Geol.*, *30*, 377-392, 1922.
White, B.R., Soil transport by winds on Mars, *J. Geophys. Res.*, *84*, 4643-4651, 1979.
White, B.R., Venusian saltation, *Icarus*, *46*, 226-232, 1981.
White, B.R., and J.C. Schultz, Magnus effect on saltation, *J. Fluid Mech.*, *81*, 497-512, 1977.
White, B.R., J.D. Iversen, R. Greeley, and J.B. Pollack, Particle motion in atmospheric boundary layers of Mars and Earth, *NASA Tech. Memo.*, *X-62463*, 200 pp., 1975.
White, B.R., R. Greeley, J.D. Iversen, and J.B. Pollack, Estimated grain saltation in a Martian atmosphere, *J. Geophys. Res.*, *81*, 5643-5650, 1976.
White, B.R., R.N. Leach, R. Greeley, and J.D. Iversen, Saltation threshold experiments conducted under reduced gravity conditions, paper AIAA-87-0621, presented at 25th Aerospace Science Meeting, Am. Inst. of Aeron. and Astron., Reno, Nev., 1987.
Woodside, W., and J.H. Messmer, Thermal conductivity of porous media, I, Unconsolidated sands, *J. Appl. Phys.*, *32*, 1688-1699, 1961.
Zimbelman, J.R., Geologic interpretation of the remote sensing data for the Martian volcano Ascraeus Mons, Ph.D. dissertation, Ariz. State Univ., Tempe, 1984. (Also in Advances in Planetary Geology, vol. 1, *NASA Tech. Memo.*, *TM-88784*, pp. 271-572, 1986.)
Zimbelman, J.R., Surface properties of the Pettit wind streak on Mars: Implications for sediment transport, *Icarus*, *66*, 83-93, 1986.
Zimbelman, J.R., Spatial resolution and the geologic interpretation of Martian morphology: Implications for subsurface volatiles, *Icarus*, *71*, 257-267, 1987.
Zimbelman, J.R., and L.A. Leshin, A geologic evaluation of thermal properties for the Elysium and Aeolis Quadrangles of Mars, *Proc. Lunar Planet. Sci. Conf. 17th, Part 2, J. Geophys. Res.*, *92*, suppl., E588-E596, 1987.

P.R. Christensen and K.S. Edgett, Department of Geology, Arizona State University, AZ 85287-1404.

(Received July 16, 1991;
revised September 9, 1991;
accepted September 19, 1991.)